Mutations in *MME* Cause an Autosomal-Recessive Charcot–Marie–Tooth Disease Type 2

Yujiro Higuchi, MD,[1] Akihiro Hashiguchi, MD, PhD,[1] Junhui Yuan, MD, PhD,[1] Akiko Yoshimura, MPAS,[1] Jun Mitsui, MD, PhD,[2] Hiroyuki Ishiura, MD, PhD,[2] Masaki Tanaka, MD, PhD,[2] Satoshi Ishihara, MD,[1,3] Hajime Tanabe, MD,[1] Satoshi Nozuma, MD,[1] Yuji Okamoto, MD, PhD,[1] Eiji Matsuura, MD, PhD,[1] Ryuichi Ohkubo, MD, PhD,[1,4] Saeko Inamizu, MD,[5] Wataru Shiraishi, MD,[5] Ryo Yamasaki, MD, PhD,[5] Yasumasa Ohyagi, MD, PhD,[5] Jun-ichi Kira, MD, PhD,[5] Yasushi Oya, MD, PhD,[6] Hayato Yabe, MD, PhD,[7] Noriko Nishikawa, MD, PhD,[7] Shinsuke Tobisawa, MD, PhD,[8] Nozomu Matsuda, MD, PhD,[9] Masayuki Masuda, MD, PhD,[10] Chiharu Kugimoto, MD,[11] Kazuhiro Fukushima, MD, PhD,[12] Satoshi Yano, MD, PhD,[13] Jun Yoshimura, PhD,[14] Koichiro Doi, PhD,[14] Masanori Nakagawa, MD, PhD,[15] Shinichi Morishita, PhD,[14] Shoji Tsuji, MD, PhD,[2] and Hiroshi Takashima, MD, PhD[1]

Objective: The objective of this study was to identify new causes of Charcot–Marie–Tooth (CMT) disease in patients with autosomal-recessive (AR) CMT.
Methods: To efficiently identify novel causative genes for AR-CMT, we analyzed 303 unrelated Japanese patients with CMT using whole-exome sequencing and extracted recessive variants/genes shared among multiple patients. We performed mutation screening of the newly identified membrane metalloendopeptidase (*MME*) gene in 354 additional patients with CMT. We clinically, genetically, pathologically, and radiologically examined 10 patients with the *MME* mutation.
Results: We identified recessive mutations in *MME* in 10 patients. The *MME* gene encodes neprilysin (NEP), which is well known to be one of the most prominent beta-amyloid (Aβ)-degrading enzymes. All patients had a similar pheno-

View this article online at wileyonlinelibrary.com. DOI: 10.1002/ana.24612

Received Oct 13, 2015, and in revised form Jan 16, 2016. Accepted for publication Feb 3, 2016.

Address correspondence to Dr Hiroshi Takashima, Department of Neurology and Geriatrics, Kagoshima University Graduate School of Medical and Dental Sciences, 8-35-1 Sakuragaoka, Kagoshima City, Kagoshima, Japan 890-8520. E-mail: thiroshi@m3.kufm.kagoshima-u.ac.jp

From the [1]Department of Neurology and Geriatrics, Kagoshima University Graduate School of Medical and Dental Sciences, Kagoshima, Japan; [2]Department of Neurology, Graduate School of Medicine, The University of Tokyo, Tokyo, Japan; [3]Department of Cardiovascular medicine, Nephrology and Neurology, Graduate School of Medicine, University of the Ryukyus, Okinawa, Japan; [4]Department of Neurology, Fujimoto General Hospital, Miyazaki, Japan; [5]Department of Neurology, Neurological Institute, Graduate School of Medical Sciences, Kyushu University, Fukuoka, Japan; [6]Department of Neurology, National Center Hospital, National Center of Neurology and Psychiatry, Tokyo, Japan; [7]Department of Neurology and Clinical Pharmacology, Ehime University Graduate School of Medicine, Ehime, Japan; [8]Department of Neurology, Tokyo Metropolitan Neurological Hospital, Tokyo, Japan; [9]Department of Neurology, Fukushima Medical University, Fukushima, Japan; [10]Department of Neurology, Tokyo Medical University, Tokyo, Japan; [11]Department of Neurology and Stroke Medicine, Yokohama City University, Yokohama, Japan; [12]Department of Home-Care Promotion, Shinshu University School of Medicine, Matsumoto, Japan; [13]Department of Neurology, Showa University School of Medicine, Tokyo, Japan; [14]Department of Computational Biology and Medical Sciences, Graduate School of Frontier Sciences, The University of Tokyo, Chiba, Japan; and [15]Director of North Medical Center, Kyoto Prefectural University of Medicine, Kyoto, Japan.

Additional supporting information can be found in the online version of this article.

type consistent with late-onset axonal neuropathy. They showed muscle weakness, atrophy, and sensory disturbance in the lower extremities. All the *MME* mutations could be loss-of-function mutations, and we confirmed a lack/decrease of NEP protein expression in a peripheral nerve. No patients showed symptoms of dementia, and 1 patient showed no excess Aβ in Pittsburgh compound-B positron emission tomography imaging.
Interpretation: Our results indicate that loss-of-function *MME* mutations are the most frequent cause of adult-onset AR-CMT2 in Japan, and we propose that this new disease should be termed AR-CMT2T. A loss-of-function *MME* mutation did not cause early-onset Alzheimer's disease. Identifying the *MME* mutation responsible for AR-CMT could improve the rate of molecular diagnosis and the understanding of the molecular mechanisms of CMT.

ANN NEUROL 2016;79:659–672

Charcot–Marie–Tooth (CMT) disease is one of the most common inherited peripheral neuropathies (IPNs), and it is clinically and genetically heterogeneous. To date, >100 different genes have been identified as disease-causing genes for CMT and other IPNs. Among them, >20 genes, such as *COX6A1*, *C12orf65*, *EGR2*, *FGD4*, *FIG4*, *GALC*, *GAN*, *GDAP1*, *HINT1*, *HK1*, *LMNA*, *MED25*, *MTMR2*, *MTMR5*, *NDRG1*, *PRX*, *SACS*, *SBF1*, *SBF2*, *SH3TC2*, *SURF1*, and *TRIM2*, have been shown to be involved in autosomal-recessive (AR) CMT (AR-CMT) or other AR-IPNs, and could be categorized into various groups based on their subcellular localization and functions.[1,2] Although a genetic diagnosis has been achieved in more than half of all patients with CMT, the molecular diagnosis rate of patients with AR-CMT is extremely low compared with that of patients with autosomal-dominant (AD) CMT, particularly that of CMT1.[3–5] This suggests the presence of causative genes that have yet to be determined and the necessity to study them further, which may result in a better understanding of CMT pathogenesis.

In this study, we attempted to identify novel AR-CMT disease-causing genes using whole-exome sequencing (WES) analyses in many patients with CMT with an overlap-based strategy, which helps identify candidate genes by focusing on variants shared among multiple unrelated patients with the same phenotype.

We identified mutations in the membrane metalloendopeptidase (*MME*) gene in 10 unrelated patients with adult-onset axonal neuropathy. The *MME* gene encodes neprilysin (NEP), which is termed cluster of differentiation 10 (CD10), and may play a role in degrading a variety of neuropeptides. NEP has been found not only in the central nervous system (CNS), but also the peripheral nervous system (PNS) in mammals.[6,7] The role of NEP in PNS is unclear; however, it is well known that NEP is one of the most prominent β-amyloid (Aβ)-degrading enzymes in the CNS.[8] NEP is recognized to play an important protective role against Alzheimer's disease.[9–11] NEP-deficient mice showed increased Aβ accumulation in the brain, which resulted in Alzheimer's disease–like pathology and behavioral abnormalities.[12,13] However, it is not yet clear how loss-of-function mutations in *MME* affect the human phenotypes.

Here, we describe the clinical characteristics of patients with CMT with *MME* mutations, including whether or not they show evidence of Alzheimer's disease, and we provide genetic and histopathological data to support the contention that the recessive mutations in *MME* are responsible for CMT.

Subjects and Methods

A total of 726 Japanese patients with clinically diagnosed CMT were enrolled in this study. However, demyelinating patients whose *PMP22* duplication or deletion were confirmed using fluorescence in situ hybridization or multiplex ligation probe amplification were not enrolled. The protocol was reviewed and approved by the institutional review board of Kagoshima University (Kagoshima, Japan). All patients and family members provided written informed consent to participate in this study.

Patient Selection of Original Study for WES

To identify novel AR-CMT disease-causing genes using WES analyses, we collected DNA samples in a first case series of 372 Japanese patients with clinically diagnosed CMT between April 2007 and April 2012. Subsequently, we excluded 69 patients with pathogenic mutations in the 28 genes known to cause CMT or IPN (Supplementary Table 1), which were detected using the custom MyGeneChip CustomSeq Resequencing Array (Affymetrix, Inc., Santa Clara, CA) following the protocol described previously.[14–17] We performed WES in the remaining 303 patients and excluded 85 patients with pathogenic mutations in the known CMT genes and in other IPN genes (Supplementary Table 1). We also excluded 55 patients suspected of AD or X-linked inheritance pattern on the basis of family history information as well as undetermined inheritance. After these exclusions, we selected 163 unrelated patients with presumed AR inheritance or with sporadic inheritance and no known genetic etiology (Fig 1).

Patient Selection of Additional Study

To investigate whether *MME* mutations cause CMT and to investigate the frequency of patients with *MME* mutations, we further performed targeted resequencing using next-generation sequencing (NGS) in a 137 second case series between May 2012 and June 2014 and a 217 third case series of unrelated Japanese patients with CMT between July 2014 and March 2015 (Fig 2).

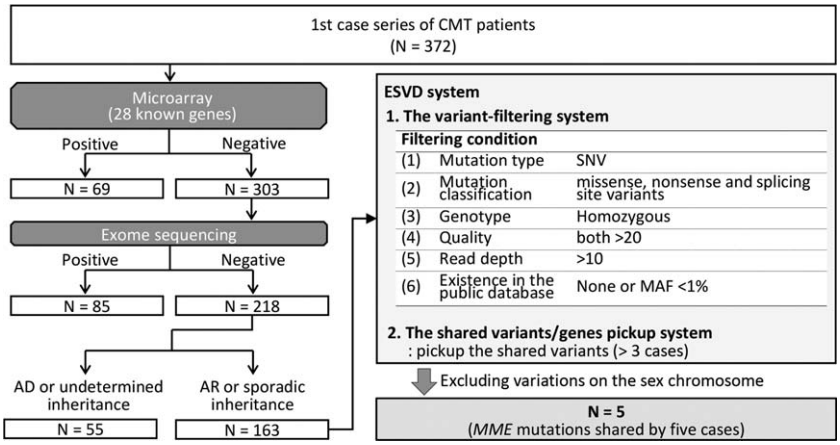

FIGURE 1: Flow chart for genetic tests, selection of patients, and exome-based shared variants detection (ESVD) system among the first case series of 372 Charcot–Marie–Tooth (CMT) patients, we selected 163 patients with presumed autosomal-recessive or sporadic CMT and no known genetic etiology. Using the ESVD system, we automatically performed variant filtering under the conditions (1) to (6). Subsequently, we identified 5 patients with a mutation in the *MME* gene by the shared variants/genes pickup system. AD = autosomal-dominant; AR = autosomal-recessive; SNV = single-nucleotide variation; MAF = minor allele frequency.

Extraction of Genomic DNA

Genomic DNA of the patients and family members was extracted from peripheral blood using QIAGEN's Puregene Core Kit C (QIAGEN, Valencia, CA) or from saliva using the Oragene DNA self-collection kit (DNA Genotech, Ottawa, Ontario, Canada), according to the manufacturer's protocol.

WES

Three micrograms of genomic DNA were processed using a SureSelect v4+UTRs or v5+UTRs kit according to the manufacturer's instructions. Captured DNA was sequenced using a HiSeq 2000 (Illumina, San Diego, CA). Sequences were aligned to the human reference genome (NCBI37/hg19) using the Burrows–Wheeler Aligner.[18] Variant calling was performed using SAMtools.[19] Variants were annotated using in-house scripts, which provided the variants list. Previously known variants were annotated from the 1000 Genomes Project and dbSNP137.

Development of the Exome-Based Shared Variants Detection System

To extract candidate genes or variants from the WES data, Maze Inc. (Tokyo, Japan) developed user-friendly analysis software, called the exome-based shared variants detection (ESVD) system, under our supervision. This system consists of two parts: a "variant-filtering system" and a "shared variants/genes pickup system." The variant-filtering system provides users with many options for filtering the raw variant data. The conditions for filtering variants include mutation type, genotype, quality, read depth, minor allele frequency (MAF), and presence in public databases; dbSNP137, 1000 Genomes project database (http://browser.1000genomes.org), and The Human Genetic Variation Database (HGVD) comprised of exome sequencing of 1,208 Japanese individuals (http://www.genome.med.kyoto-u.ac.jp/SnpDB/). Moreover, the shared variants/genes pickup system allowed us to detect the variants and genes shared among cases with similar phenotypes, and the number can be custom defined. In this study, using the ESVD system, we automatically performed variant filtering under the following conditions: (1) mutation type (single-nucleotide variation [SNV]; not including insertion and deletion); (2) mutation classification (nonsynonymous, nonsense, and splicing site variants); (3) genotype (homozygous); (4) Phred-scaled quality score/mapping quality (both >20); (5) read depth (> 10); and (6) existence in the public database (none or MAF <1%). Subsequently, we manually selected the variants on an autosome. Eventually, after filtering, the variants that were shared by three or more cases were extracted (Fig 1). We also manually extracted presumed compound heterozygous variants of the *MME* gene from the WES data set of the 163 patients.

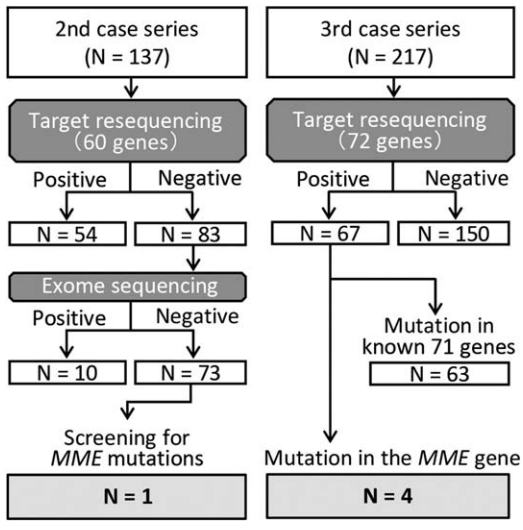

FIGURE 2: Flow chart for genetic tests in the additional patients. During the second and third case series, we identified 1 and 4 patients with mutations in the *MME* gene.

Mutation Screening of the MME *Gene in the Additional Patients*

For the second series, we performed mutation screening of 60 known or candidate CMT-related genes using the Illumina Miseq platform (Illumina Inc., San Diego, CA, USA) following the protocol described previously by Maeda et al.[20] Subsequently, we performed mutation screening of other known CMT and IPN genes, including the *MME* gene, using WES (Fig 2). For the third series, we performed targeted resequencing of 72 known or candidate CMT-related genes, including the *MME* gene, using a custom Ion AmpliSeq^{M} panel (Life Technologies, Carlsbad, CA) (Fig 2 and Supplementary Table 1). Briefly, a custom panel targeting 72 genes was designed using the Ion AmpliSeq Designer tool (http://www.ampliseq.com). Library and template preparation was performed according to manufacturer's instructions. Sequencing was performed on the Ion Proton (Life Technologies) using the Ion PI Chip kit v2 BC. Sequence data were aligned and mapped to the reference sequence, and variants were called using the Torrent variant caller. Variants were transferred to the CLC Genomics Workbench 6 software program (CLC bio, Aarhus, Denmark) for annotation and filtering.

Mutation Confirmation and Segregation Analysis

Using Sanger sequencing, we reconfirmed the pathogenic mutations revealed by microarray or NGS. Furthermore, segregation studies were performed in the available family members whenever possible. In order to rule out the possibility that the prioritized variants in the *MME* gene may be Japanese-specific polymorphisms, we confirmed whether the variants that existed in the in-house database comprised of the WES data from 800 Japanese healthy control subjects and 3,742 disease control subjects excluding patients with CMT.

In Silico Analysis

To determine whether variants in the *MME* gene are damaging or deleterious, we obtained the predicted functional scores of nonsynonymous variants or deletions with three prediction algorithms, including PolyPhen2,[21] SIFT (Sorts Intolerant From Tolerant amino acid substitutions),[22] and PROVEAN (Protein Variation Effect Analyzer).[23]

RNA Extraction and Reverse-Transcription Polymerase Chain Reaction

To study the messenger RNA (mRNA) expression of the *MME* gene, we performed reverse-transcription polymerase chain reaction (RT-PCR) in individuals from some families with *MME* mutations. Whole blood was collected into PAXgene Blood RNA Tubes (Qiagen), and total RNA was prepared from blood using the PAXgene Blood RNA Kit (Qiagen) in order to generate a complementary DNA (cDNA) pool by RT-PCR using the High-Capacity cDNA Reverse Transcription Kit (Applied Biosystems, Carlsbad, CA), according to the manufacturer's instructions. PCR primers for the β-actin housekeeping gene were used as the internal control. *MME* cDNAs were amplified using the following primer pairs: (1) forward primer located in exon 6: 5′-TGATAGCAGAGGTGGAGAACC-3′ and reverse primer in exon 9: 5′-CATCGATGGGCAATCTTTCT-3′; (II) forward primer in exon 4: 5′-AATGTCATTCCCGAGACC AG-3′, reverse primer in exon 7: 5′-TCATCAGTGCCAACAA ACAA-3′. The expected sizes of the RT-PCR products were 350bp (base pairs) and 344bp for primer pairs 1 and 2, respectively. PCR products were subjected to agarose gel electrophoresis and sequenced using the Sanger method.

Haplotype Analyses

To determine whether recurring *MME* mutations (c.654+1G>A) occurred because of independent mutational events or common ancestry, we performed a haplotype analysis using five microsatellite markers (D3S1595, D3S1280, D3S3509, D3S1275, and D3S3692) and seven single-nucleotide polymorphisms (SNPs; rs1803155, rs12493885, rs12497267, rs9438, rs358733, rs11918974, and rs3816527) flanking the *MME* gene by an automated fluorescent method on an ABI 3130xL or 3500xL genetic analyzer (Applied Biosystems).

Cognitive Assessment and Neuroimaging

In some patients, we performed brain magnetic resonance imaging (MRI) or computed tomography (CT), and a neuropsychological examination including the Mini–Mental State Examination (MMSE; 0–30 scale, normal >24)[24] and the Alzheimer's Disease Assessment Scale-Cognitive Behavior Section (ADAS-cog; 0–70 scale, normal <10).[25] We also evaluated patient 1 (P1) with amyloid positron emission tomography (PET) imaging with ^{11}C-PIB (Pittsburgh compound-B). PET data were acquired on a Discovery PET/CT 710 (GE Healthcare, Tokyo, Japan) after the injection of ^{11}C-PiB (470 MBq). ^{11}C-PiB images were derived from dynamic summations of standard uptake values (SUVs) over 60 minutes and were normalized with the cerebellum as a reference region (SUVR).

Histopathological Examinations

Sural nerve biopsies obtained from P1 and P4 were analyzed for morphometric changes using light microscopes. Semithin sections from Epon embedded tissues were stained with Toluidine blue. An immunohistochemical assay was performed using an anti-NEP/CD10 antibody (ab951; Abcam, Tokyo, Japan) in tissue from human tonsils and peripheral nerves, and the findings were compared to a disease control patient (female, 39 years old, polymyositis).

Western blotting

Western blotting was performed using sodium dodecyl sulfate/polyacrylamide gel electrophoresis. Briefly, 20-μg homogenates of sural nerve were resuspended in a reduced sample buffer, electrophoresed on a 10% Tris gel with Tris running buffer, blotted to a polyvinylidene difluoride membrane, and sequentially probed with polyclonal rabbit antihuman CD10 antibody (Abcam). The membrane was subsequently incubated with a horseradish peroxidase–labeled polymer-conjugated antimouse

TABLE. Genetic, Clinical, and Laboratory Findings

Patient No.	P1	P2	P3	P4	P5	P6	P7	P8	P9	P10
Mutation	c.654+1G>A (p.Gly179fs)	c.654+1G>A (p.Gly179fs)	c.654+1G>A (p.Gly179fs)	c.1861T>C (p.Cys621Arg)	c.661C>T (p.Gln221X)	c.1231_1233delTGT (p.Cys411del)	c.439+2T>A (p.exon5del)	c.439+2T>A (p.exon5del) c.655−2A>G (p.exon8del)	c.1817G>A (p.Trp606X)	c.655−2A>G (p.exon8del)
Genotype	Hmz	Hmz	Hmz	Hmz	Hmz	Hmz	Hmz	CH	Hmz	Hmz
Classification	Splice	Splice	Splice	Missense	Nonsense	Deletion	Splice	Splice	Nonsense	Splice
Sex/age, yr	M/67	M/49	M/59	M/66	M/58	F/65	M/73	M/51	M/54	F/47
Onset age, yr	54	36	50	56	48	54	50	47	40	37
Inheritance pattern	AR	AR	AR	AR	AR	AR	AR	AR/sporadic	AR	AR
Consanguinity	+	+	−	+	+	−	+	−	−	+
Initial symptom[a]	Motor	Motor	Motor	Motor	Motor	Motor	Motor	Sensory	Motor	Sensory
MMT[b]	1	2	1	3	3	2	4	4	1	3
Sensory disturbance	+	+	+	+	+	−	+	+	+	+
Decreased DTRs	+	+	+	+	+	+	+	+	+	+
Dementia	−	−	NA	−	−	−	−	−	−	−
MMSE	29	30	NA	29	28	29	26	30	28	30
Brain atrophy[c]	−	NA	NA	−	−	NA	NA	−	NA	−
Type	Ax	Ax	Ax	Ax	De/Ax	Ax	Ax	Ax	Ax	Ax
NCS[d] DL	3.2	4.3	3.6	6.3	4.3	3.3	4.5	4.6	3.6	3.5
dCMAP	6.4	4.5	10	3.2	4.5	6.9	8.2	1.7	4.7	7.3
MCV	47.5	42.8	53	45.5	37.4	45.1	41.3	39.2	45	42

[a]'Motor' indicates distal lower limbs weakness/atrophy or gait disturbance, and 'Sensory' indicates decreased superficial sensation or dysesthesia in lower limbs.
[b]Scores indicating manual muscle testing (MMT) grade in the distal lower limbs.
[c]Brain atrophy is evaluated by CT or MRI.
[d]Nerve conduction study of Median nerve.
Ax = axonal; CH = compound heterozygous; CT computed tomography; dCMAP = distal compound muscle action potential (mV); De = demyelinating; DL = distal latency (ms); DTRs = deep tendon reflexes; Htz = heterozygous; Hmz = homozygous; MCV = motor conduction velocity (m/s); MMSE = Mini–Mental State Examination; MRI = magnetic resonance imaging; NA = not available (not scored or not examined); NCS = nerve conduction study.

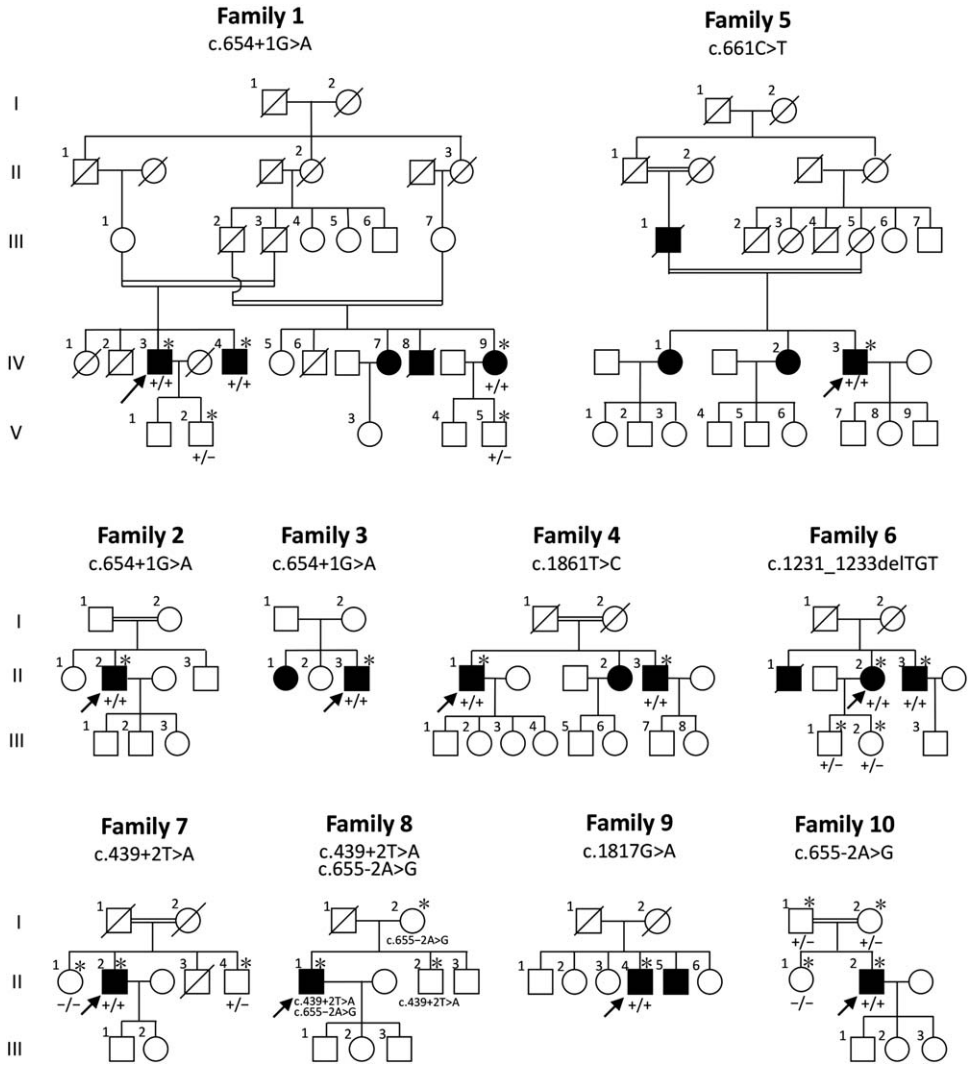

FIGURE 3: Pedigrees and segregation analysis of *MME* mutations in 10 families. P1, P2, P4, P5, P7, and P10 have consanguineous parents. P3, P6, and P9 have unaffected parents with affected siblings, and P8 was sporadic. Autosomal-recessive inheritance is presumed in all pedigrees. A DNA sample was available from individuals marked with an asterisk. Affected members have a homozygous or compound heterozygous mutation, whereas unaffected members were heterozygous or wild-type carriers. Squares represent males and circles represent females. Filled symbols represent those affected with a similar phenotype. Oblique lines represent deceased family members. Black arrows indicate the proband (P1–P10). +/+ = homozygous for mutation; +/− = heterozygous; −/− = homozygous for wild type.

antibody reagent (EnVision+ reagent; Dako, Tokyo, Japan). 3-3′-diaminobenzidine was used for chromogenic visualization.

Results

Identification of MME *Mutations*

Figure 1 shows a flow chart for the selection of patients, genetic tests, and the filtering process for homozygous variants using the ESVD system. We extracted three kinds of homozygous mutations in the *MME* gene in 5 patients in the first case series of patients with CMT with no pathogenic mutations in known CMT or IPN genes. In P1 to P3, we identified the same homozygous mutation in the splice donor site [c.654+1G>A] in intron 7 of *MME*. A novel homozygous missense mutation [c.1861T>C, p.Cys621Arg] and a nonsense mutation [c.661C>T, p.Gln221X] were found in P4 and P5, respectively. On the other hand, we could not extract presumed compound heterozygous variants or other homozygous variants in *MME* from the WES data of 163 AR/sporadic cases in first case series, although we identified a novel heterozygous nonsense variant of unknown significant (c.264C>A, p.Cys88X) and a rare SNV (c.1489T>C, p.Typ497His). In the second and third case series of patients with CMT with no pathogenic mutations in known CMT or IPN genes, five additional recessive mutations in the *MME* gene were identified (Fig 2): [c.1231_1233delTGT, p.Cys411del], [c.439+2T>A], [c.439+2T>A and c.655−2A>G

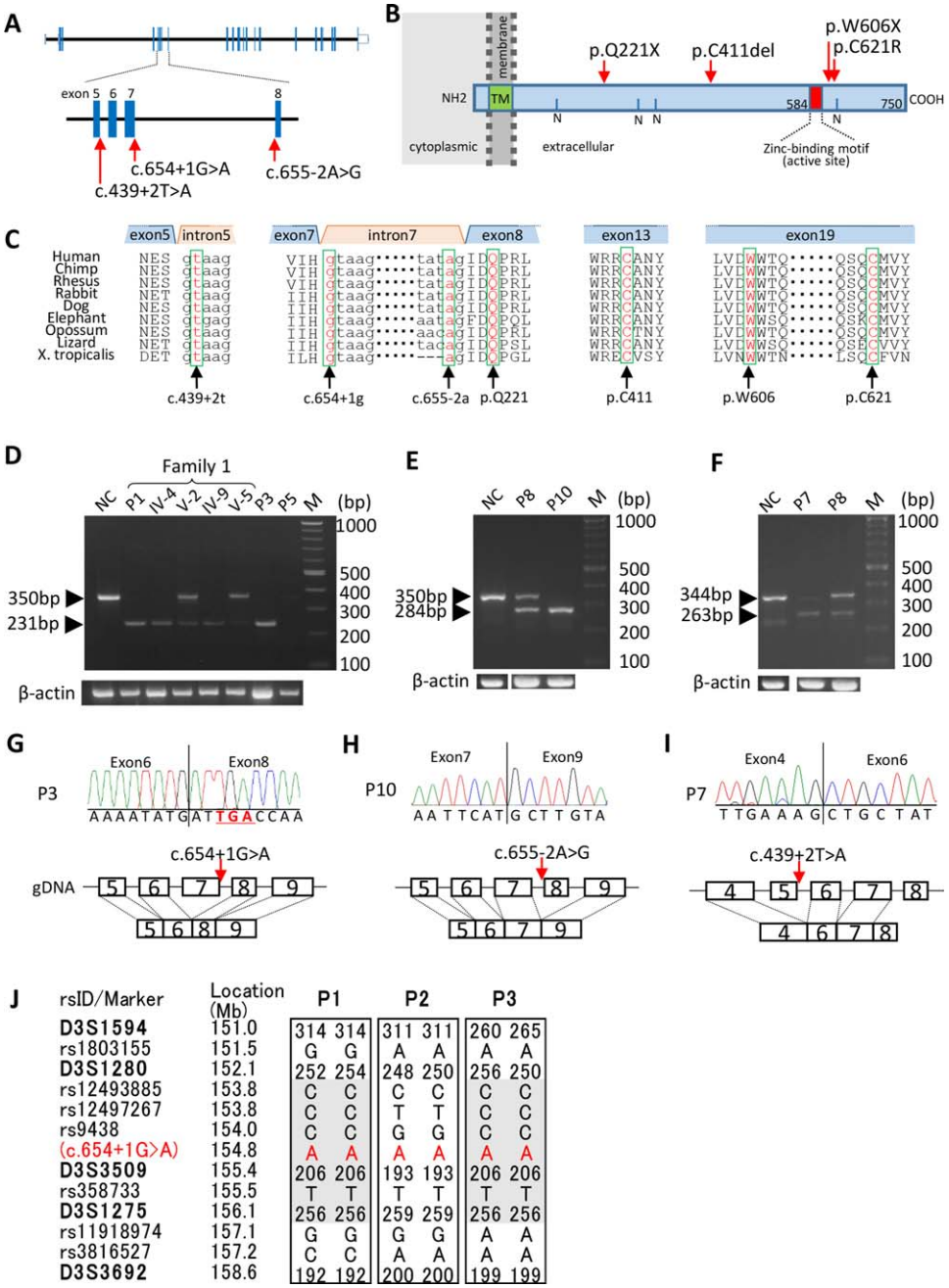

J

rsID/Marker	Location (Mb)	P1		P2		P3	
D3S1594	151.0	314	314	311	311	260	265
rs1803155	151.5	G	G	A	A	A	A
D3S1280	152.1	252	254	248	250	256	250
rs12493885	153.8	C	C	C	C	C	C
rs12497267	153.8	C	C	T	T	C	C
rs9438	154.0	C	C	G	G	C	C
(c.654+1G>A)	154.8	A	A	A	A	A	A
D3S3509	155.4	206	206	193	193	206	206
rs358733	155.5	T	T	T	T	T	T
D3S1275	156.1	256	256	259	259	256	256
rs11918974	157.1	G	G	G	G	A	A
rs3816527	157.2	C	C	A	A	A	A
D3S3692	158.6	192	192	200	200	199	199

FIGURE 4: Localization and conservation of *MME* mutations, haplotype analysis, and RNA analysis. (A and B) Schematic representation of the *MME* gene and neprilysin. Red arrows indicate the location of mutations in the extracellular domain. N = N-glycosylation sites; TM = transmembrane domain. (C) Conservation analysis. Glutamine 221, cysteine 411, tryptophan 606, cysteine 621, and canonical GT-AG nucleotides (c.439+2t, c.654+1g, c.655-2a) of the splice donor and acceptor junctions in the *MME* gene were highly conserved among species. (D) Agarose gel electrophoresis of cDNA fragments obtained from RT-PCR of P1, his family member (IV-4, V-2, IV-9, and V-5), P3 with the c.654+1G>A mutation, P5 with c.661C>T mutation, and a normal control (NC). The P1, IV-4 (affected), IV-9 (affected), and P3 lanes showed a 231-bp band, which is smaller than the 350-bp band in the NC lane. The V-2 and V-5 (unaffected heterozygous carrier) lanes showed a 231-bp band and a 350-bp band. The P5 lane showed no band. (E) Agarose gel electrophoresis of cDNA fragments obtained from RT-PCR of P8, P10 with the c.655-2A>G mutation, and the NC. The P10 lane showed a 284-bp band, which is smaller than the 350-bp band in the NC lane. The P8 lane showed a 284-bp band and a 350-bp band. (F) Agarose gel electrophoresis of cDNA fragments obtained from RT-PCR of P7, P8 with the c.439+2T>A mutation, and the NC. The P7 lane showed a 263-bp band, which is smaller than the 344-bp band in the NC lane. The P8 lane showed a 263-bp band and a 344-bp band. (G– I) Sequence chromatogram of the RT-PCR product from P1, P10, and P7 showing exon 7 skipping and premature termination within exon 8 (G), exon 8 skipping (H), and exon 5 skipping (I) as schematically shown in the lower panel, respectively. (J) Haplotype analysis in P1 to P3. Shared haplotypes are shown in the gray box.

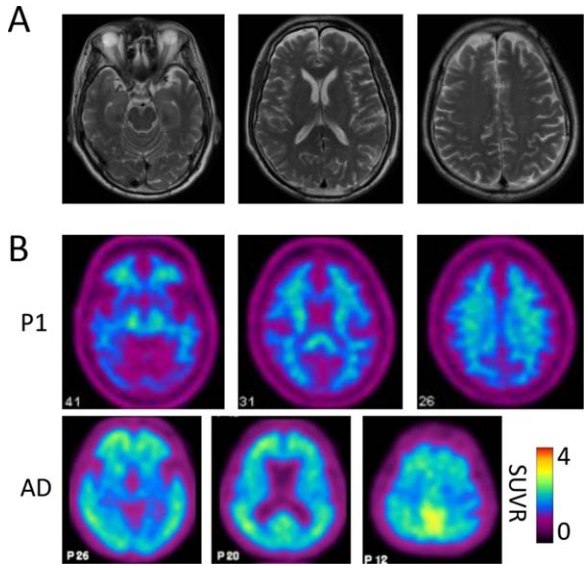

FIGURE 5: Magnetic resonance imaging and Pittsburgh compound-B (PiB) positron emission tomography imaging. (A) T2-weighted images of P1 showing no significant brain atrophy at 67 years of age. (B) PiB standardized uptake value (SUV) images of PiB retention in P1 at 67-years of age and a ^{11}C-PiB-positive Alzheimer's disease patient. Images from P1 show a lack of PiB retention throughout the gray matter and nonspecific PiB retention in the white matter compared with that of the patient with Alzheimer's disease, which shows a high retention of PiB throughout the gray matter. SUVR = standardized uptake value retention.

(compound heterozygous mutation)], [c.1817G>A, p.Trp606X], and [c.655−2A>G] mutations in P6 to P10, respectively (Table). Segregation analysis from the families of P1, P4, P6, P7, P8, and P10 revealed that the *MME* mutations were segregated with the disease in each family (Fig 3). Glutamine 221, cysteine 411, tryptophan 606, cysteine 621, and canonical GT-AG nucleotides of the splice donor and acceptor junctions in the *MME* gene were highly conserved among species (Fig 4A–C). Notably, the p.Cys621Arg mutation was classified as "pathogenic" or "deleterious" using in silico analysis (Polyphen2 score = 1.00, SIFT score = 0.00, and PROVEAN score = −11.2 [cutoff = −2.5]), and the p.Cys411del mutation was also predicted as deleterious in the PROVEAN software (PROVEAN score = −17.4 [cutoff = −2.5]). MAF of all the validated mutations in public databases, including Exome Sequencing Project (ESP) and Exome Aggregation Consortium (ExAC), and in-house database was ≤0.002 (Supplementary Table 2).

Clinical Features of 10 Unrelated Patients With MME *Mutations*

P1, a 67-year-old man born to healthy consanguineous parents, had no relevant medical history. At aged 54 years, he first noticed that his flip-flops slipped off easily because of foot drop and subsequently developed a slowly progressive gait disturbance and dysesthesia of the lower limbs. Neurological examination revealed severe weakness and atrophy of the distal limb muscles, especially the bilateral tibialis anterior muscles, which was grade 1 on the Medical Research Council scale.[26] Superficial and deep sensations were decreased in the lower limbs. The cranial nerves were normal. Nerve conduction studies (NCSs) showed an axonal type of motor and sensory neuropathy: mild slowing of conduction velocity (> 38 m/s) in the median and ulnar nerve, and absent motor and sensory responses in the lower extremities (Table). On the basis of these findings, he was diagnosed with an autosomal recessively inherited axonal form of CMT. He had no obvious cognitive impairment; his MMSE score was 29/30 and his cognitive subscale of the Japanese version of the Alzheimer's disease assessment scale (ADAS-J-cog) score was 5/70. His brain MRI was almost normal (Fig 5A), and a PiB-PET scan did not show a significant amount of amyloid deposition (Fig 5B).

We summarized the clinical features and electrophysiological findings of all 10 patients in the Table. Mean age of onset of disease was 47.2 years (range, 36–56). Six of them were born to consanguineous parents (Fig 3). Clinically, all patients had slowly progressive weakness and atrophy of distal limb muscles, gait disturbance (but not yet become wheelchair dependent), sensory disturbance of the distal limbs, and decreased or absent tendon reflexes, all of which were the typical CMT phenotype. No patients showed additional neurological findings, such as pyramidal signs, cerebellar ataxia, and other CNS symptoms. NCSs showed an axonal sensorimotor neuropathy in all patients, except for P5 who was electrophysiologically diagnosed with a demyelinating/intermediate form based on delayed median nerve conduction velocities (37.4 m/s). Nine of the patients evaluated had no apparent cognitive impairment as assessed by the MMSE; all scored 26 or higher. The remaining patient had no subjective memory complaints and no clinically apparent cognitive impairment. MRI or CT scans did not show cerebral atrophy in the 5 patients evaluated.

RNA Expression Analysis and Haplotype Analysis of MME

RNA analysis obtained from 6 patients (P1, P3, P5, P7, P8, and P10) and a P1 family member revealed abnormal transcripts. In P1 and P3 with the c.654+1G>A mutation at the splicing donor site of intron 7 of the *MME* gene, agarose gel electrophoresis of the RT-PCR products obtained with primer pair 1 showed a band smaller than the 350-bp band observed in the healthy

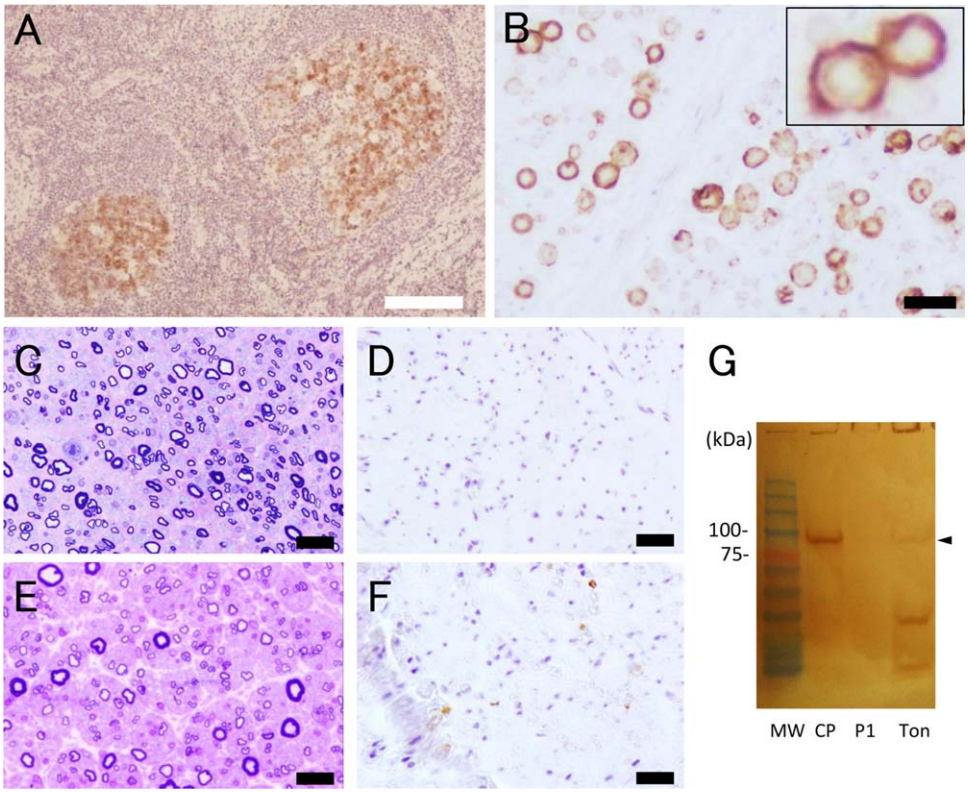

FIGURE 6: Neprilysin immunohistochemistry and western blot analysis. (A) Immunohistochemical staining with an anti-NEP/CD10 antibody revealed the expression of NEP/CD10 (brown) in the marginal center of human tonsil. (B) Expression of NEP/CD10 (brown) was observed in myelin and axons, especially at the outer surface of myelin of the sural nerve from a control patient (inset). (C and E) Toluidine blue staining of a sural nerve. Densities of large myelinated fibers are markedly decreased in both patient 1 (C) and 4 (E), who harbor the c.654+1G>A (p.Gly179fs) and c.1861T>C (p.Cys621Arg) mutation, respectively. Clusters of small myelinated fibers are occasionally noted. (D and F) Expression of NEP/CD10 (brown) was not detected in the nerve from P1 (D), but partially detected in the nerve from P4 (F). (G) Western blot analysis of NEP/CD10. Blotted bands were detected with a rabbit anti-NEP/CD10 antibody (arrowhead). NEP/CD10 was detected in homogenates from the sural nerve of the control patient, but not P1. White bar, 100 μm; black bar, 20 μm. CP = control patient; MW = molecular weight marker; P1 = patient 1; Ton = human tonsil.

normal control (NC; Fig 4D). Sequences of the RT-PCR products in P1 and P3 revealed aberrantly spliced mRNA lacking exon 7, resulting in a 231-bp fragment (Fig 4G). The lack of exon 7 creates a frameshift and, consequently, premature termination within exon 8; therefore, the c.654+1G>A mutation was designed as p.Gly179AspfsX2 at the protein level. In P5 with the c.661C>T nonsense mutation, RT-PCR products were not detected (Fig 4D), suggesting the occurrence of nonsense-mediated decay of *MME* mRNA. In P8 and P10 with the c.655−2A>G mutation at the splicing acceptor site of intron 7, the RT-PCR products showed a smaller band than the 350-bp band of the NC (Fig 4E). The sequences of the RT-PCR products in P10 revealed aberrantly spliced mRNA lacking exon 8, resulting in a 284-bp fragment (Fig 4H). The lack of exon 8 lead to an in-frame deletion of 22 amino acids from the catalytic (extracellular) domain of NEP (p.Ile219_Glu240del). In P7 and P8 with the c.439+2T>A mutation at the splicing donor site of intron 5, the RT-PCR products obtained with primer pair 2 showed a band smaller than the 344-bp band of the NC (Fig 4F). Sequences of the RT-PCR products revealed aberrantly spliced mRNA lacking exon 5, resulting in a 263-bp fragment (Fig 4I). The lack of exon 5 lead to an in-frame deletion of 27 amino acids from the catalytic domain of NEP (p.Asp120_Glu146del; Asp120Ala).

Haplotype analysis in 3 patients (P1–P3) with the same homozygous c.654+1G>A mutation revealed that P1 and P3, but not P2, shared the same haplotype for the two closest markers (D3S3509 and D3S1275) and four SNPs (rs12493885, rs12497267, rs9438, and rs358733; Fig 4J).

Histopathological Findings and Expression of NEP

An immunohistochemical assay with an anti-NEP/CD10 antibody showed expression of NEP in the germinal center of human tonsil tissue, in which NEP is highly expressed on proliferating B cells, confirming the

specificity of the antibody against NEP (Fig 6A). Using this antibody, we confirmed the obvious expression of NEP in the myelin sheath of the sural nerve from the control patient, although it was also slightly expressed in the axon (Fig 6B). We obtained sural nerve biopsies from P1 and P4. Both showed a remarkable decrease in the density of large myelinated fibers with thin myelin sheaths and clusters of myelinated fibers (Fig 6C,E). Inflammatory cells and onion-bulb formation were absent. Immunohistochemical staining with an anti-NEP/CD10 antibody showed a negative and a partial positive reaction in P1 and P4, respectively, compared to myelin of the sural nerve from the control patient (Fig 6D,F). In addition, the antibody detected a band migrating at approximately 90kDa, corresponding to NEP, in the homogenates from the sural nerve of the control patient by western blotting, but the band was not detected in P1 (Fig 6G).

Discussion

We performed WES in 303 unrelated Japanese patients with CMT among a first case series and successfully identified the *MME* gene as a novel AR-CMT disease-causing gene using an overlap-based strategy. After mutation screening analyses on *MME* in a second and third case series of unrelated patients, we finally identified mutations in the *MME* gene in 10 unrelated patients with CMT. WES is one of the most effective methods for identifying pathogenic mutations in Mendelian disorders.[27–29] Abundant bioinformatic tools that efficiently prioritize pathogenic mutations or strategies that find disease-causing genes have been developed. Three main analytical strategies—linkage-based, de novo–based, or overlap-based strategies—are widely used for gene research after WES.[30,31] The overlap-based strategy helps to identify candidate genes by focusing on variants shared among multiple unrelated patients. The ESVD system we have developed based on this strategy is capable of simultaneously executing variant filtering and detecting the variants shared by disease samples and consequently contributed to the identification of the *MME* gene. This system could effectively identify novel causative genes in other Mendelian disorders.

Our study revealed various recessive *MME* mutations: nonsense, missense, splice site, and deletion. The results of the RNA analysis obtained from patients with the splice site or nonsense mutations demonstrated aberrant splicing or lack of RT-PCR fragments, respectively. Moreover, we confirmed the complete absence of detectable NEP by immunohistochemical and western blotting in the sural nerve of P1 with the c.654+1G>A mutation. These findings suggest that these mutations lead to a lack of NEP protein expression in the PNS attributed to a premature stop codon or nonsense-mediated mRNA decay. Similarly, two nonsense mutations (p.Gln221X and p.Trp606X) may cause nonsense-mediated mRNA decay. A missense mutation (p.Cys621Arg) in P4 was predicted to be damaging during in silico analysis, and cysteine 621 was highly conserved across species. Expression of NEP in the sural nerve was partially reduced. These findings suggest that this missense mutation may lead to abnormal axonal transport or fast degradation of the mutated protein. The 3-bp in-frame deletion (c.1231_1233delTGT) that eliminates cysteine at codon 411 was predicted to be deleterious using in silico analysis, and cysteine 411 was also highly conserved across species, suggesting that this deletion may affect the function of NEP. The c.439+2T>A and c.655−2A>G mutation causing in-frame exon skipping may lead to the large structural alterations and affect the expression and function of NEP. Taken together, our results suggest that all the recessive *MME* mutations in these 10 unrelated patients with CMT could be loss-of-function mutations, although the effects of expression and function of NEP on some mutations (c.1231_1233delTGT, c.439+2T>A, and c.655−2A>G) need further analysis. The result of the haplotype analysis that P1 and P3 shared the same haplotype indicates a possible ancestral founder effect for the c.654+1G>A mutation. In contrast, P2 did not share this particular haplotype and an MAF of this variation in the HGVD database is 0.002 (genotype count: G/G = 299, G/A = 1, and A/A = 0), suggesting that the mutation results from independent mutational events.

Clinically, all the patients with the *MME* mutation had a similar clinical and electrophysiological phenotype consistent with a late-onset axonal-type motor and sensory neuropathy. Although 1 patient (P5) had borderline motor nerve conduction velocity (NCV; 37.4 m/sec) of the median nerve between demyelinating and axonal form, we considered that his NCSs showed a primary axonal neuropathy with secondary demyelination because motor NCV of the ulnar nerve was 45.5 m/sec (>38 m/sec) and compound muscle action potential (CMAP) and sensory nerve action potential (SNAP) in the lower limb nerves were not evoked. In 2 patients, larger myelinated fibers were markedly decreased in peripheral nerves, and occasionally thin myelin sheaths without onion-bulb formation were present, suggesting that the pathological process is primarily axonal degeneration.

The human *MME* gene maps to chromosomal region 3q25.1 to q25.2, is composed of 24 exons, and is highly conserved among mammalian species.[32] NEP is a type 2 MME consisting of 742 amino acids and has a

	Modes of inheritance					Total
	AD	AR	X-linked	sporadic	unknown	
Pathogenic mutation	104	17	29	115	16	**281**
***MME* mutation**	0	10	0	0	0	**10**
unknown Dx	98	50	3	267	17	**435**
Number of patients	**202**	**77**	**32**	**382**	**33**	**726**

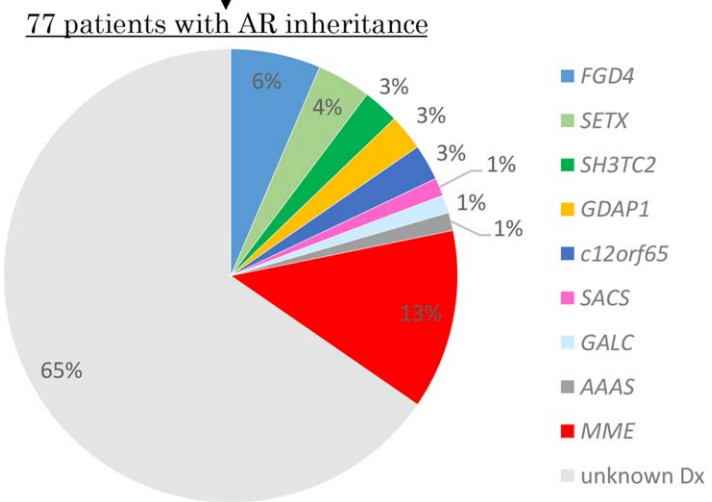

FIGURE 7: Rate of molecular diagnosis categorized according to inheritance modes. The upper table indicates the number of patients with molecular diagnoses by modes of inheritance in 726 patients. The pie chart below shows the rate of molecular diagnosis focused on the AR mode of inheritance. Only 17 of 77 (22%) patients received a molecular diagnosis in known CMT or IPN genes. Ten patients (13%) received a new molecular diagnosis, *MME* gene mutations. Rate of molecular diagnosis was increased to 35%. AR = autosomal-recessive; CMT = Charcot–Marie–Tooth; IPN = inherited peripheral neuropathy.

molecular weight ranging from 85 to 110kDa depending on differences in its glycosylation. NEP is an ectoenzyme with the bulk of its structure, including the active site, facing the extracellular space,[8] as shown Figure 4B. NEP is widely expressed in many tissues, including the nervous system,[33,34] and degrades a number of substrates such as enkephalins, substance P and atrial natriuretic peptide, and, most notably, the "Alzheimer peptide," Aβ. Moreover, *MME* is also abundantly expressed in the kidney, and previous studies have suggested that *MME* might play a role in the normal physiological function of podocytes and was involved in various renal diseases.[35,36] However, renal failure and nephrotic syndrome were not observed in 8 patients evaluated, except for 2 who had mild proteinuria (Supplementary Table 3). These data indicated that loss-of-function mutations in the *MME* gene may be not sufficient to cause congenital renal disease.

In the CNS, NEP is mainly located on neurons, particularly in the striatonigral pathway, hippocampus, and cortical regions,[37,38] and it is localized along axons and at presynaptic sites.[39] These observations suggest that after synthesis in the soma, NEP is anterogradedly transported to axon terminals, where it may play an important role in neuronal function. In general, NEP knockout mice developed normally, but showed a greater sensitivity to endotoxin shock,[40] elevated microvascular permeability,[41] enhanced aggressive behavior, and altered locomotor activity.[42] It was demonstrated that NEP knockout mice have increased levels of Aβ peptides in the brain, and administration of the NEP inhibitor, thiorphan, to rats led to increased Aβ levels.[43,44] Moreover, NEP knockout mice exhibited amyloid-like deposits with signs of neurodegeneration in the hippocampus and behavioral deficits.[13] These findings suggest that the decline of NEP is an important factor in the progression of Alzheimer's disease.[45] In contrast, Thomas et al showed that the learning abilities were not reduced in older NEP knockout mice; rather, they were significantly improved, and Aβ deposits could not be detected by immunohistochemical methods, in spite of the elevated Aβ levels in the brains of these mice.[46] In humans, no mutation in the *MME* gene linked to familial Alzheimer's disease has been reported, although some nucleotide repeat polymorphisms have been reported to be associated with susceptibility to sporadic Alzheimer's disease.[47,48] We hypothesized that human NEP deficiency would lead to cognitive impairment and increased Aβ plaque accumulation. Contrary to our expectation, neuropsychological testing revealed no obvious cognitive

deficits in 9 patients evaluated by MMSE scores. Moreover, amyloid PET imaging, which is capable of visualizing amyloid accumulation even in mild cognitive impairment or preclinical stages of Alzheimer's disease,[49] was conducted and P1 showed no obvious ^{11}C-PIB retention. These clinical data indicated that loss-of-function mutations in the human *MME* gene are not sufficient to cause early-onset familial Alzheimer's disease, and NEP deficiency may be compensated for by other Aβ-degrading enzymes, such as insulin-degrading enzyme or endothelin-converting enzyme, in vivo.[11]

In the PNS, NEP has been found in neonatal and early postnatal Schwann cells in the pig or rat sciatic nerve,[6,7] and NEP expression increased after axonal damage in adult rat Schwann cells in the sciatic nerve.[50] Although there are no reports that *MME* mutations result in peripheral neuropathy, a previous study revealed that after chronic constriction injury of the sciatic nerve, *MME* knockout mice were more sensitive to heat and mechanical stimuli than were wild-type mice, and developed edema and changes in limb temperature resembling human complex regional pain syndrome with increases in substance P and endothelin 1 in sciatic nerves.[51] Interestingly, a recent study revealed the NEP is transported by antero- and retrograde axonal flow in rat sciatic nerves.[52] In addition, our patients showed axonal neuropathy. These findings suggest that NEP could play a role in peripheral nerve development and axonal regeneration. However, as shown in Figure 6B, our immunohistochemical data revealed that NEP expression in the myelin sheath is considerably more than in the axon. For example, the mutations of peripheral myelin protein zero (*MPZ*) usually causes demyelinating neuropathy; however, sometimes axonal neuropathy phenotype is also shown, particularly in late-onset form.[53] In our study, given that all patients with *MME* mutations showed late-onset CMT, we believe that similar degeneration process may be present in both conditions by impairing Schwann cell–axonal interactions. Further studies are needed to clarify the role of *MME* in the PNS, to identify the molecular pathomechanism underlying CMT, and to develop an effective treatment for the disease.

NEP has received considerable attention as a therapeutic target for Alzheimer's disease. Fortunately, Iwata et al have successfully developed a new gene delivery system by an adeno-associated virus that can achieve comprehensive gene expression of NEP in the brain of young NEP-deficient mice, eventually decelerating Aβ accumulation and alleviating cognitive dysfunction.[54] This gene therapy may be applied for the prevention and treatment of patients with not only Alzheimer's disease, but also CMT caused by *MME* mutations in the near future.

Finally, we calculated the molecular diagnosis rate by only focusing on the AR mode of inheritance. Although only 17 of 77 (22%) patients received a molecular diagnosis by our microarray or NGS, the identification of the *MME* gene resulted in an improved molecular diagnosis rate of 35% (Fig 7). Interestingly, this result indicates that *MME* is the most frequent cause of AR-CMT2 in Japan.

In conclusion, for the first time, we identified *MME* as the most common causative gene for AR-CMT using WES followed by the ESVD system with an overlap-based strategy. Our genetic and immunohistochemical data strongly support the finding that the *MME* gene is a novel causative gene for AR-CMT. All 10 patients with the *MME* mutation had a similar phenotype with a late-onset axonal-type motor and sensory neuropathy, but with no evidence of Alzheimer's disease, and we propose this new classification as AR-CMT type 2T. Identification of the *MME* mutations responsible for AR-CMT can improve the rate of molecular diagnosis, understanding of the molecular mechanisms of CMT, and establishment of effective therapeutic approaches.

Acknowledgment

This study was supported, in part, by grants from the research on the Nervous and Mental Disorders and Research Committee for Charcot–Marie–Tooth Disease, Neuropathy, Ataxic Disease and Applying Health and Technology of Ministry of Health, Welfare and Labour, Japan. This research is also supported by the research program for conquering intractable disease from Japan Agency for Medical Research and Development (AMED).

We thank Harunobu Yunokawa and Koji Suzuki of Maze Inc. for expert bioinformatics development and support, Mrs Aya Ebina and Miho Minami of our department for her excellent technical assistance, and Enago (www.enago.jp) for the English language review. We authors thank the patients and their families for participating in this study and their physicians for submitting the clinical samples.

Author Contributions

Y.H. and H. Takashima were responsible for conception and design of the study. Y.H. and H. Takashima; acquisition and analysis of data: All authors were responsible for acquisition and analysis of data. Y.H. was responsible for writing the manuscript.

Potential Conflicts of Interest

Nothing to report.

References

1. Tazir M, Bellatache M, Nouioua S, et al. Autosomal recessive Charcot-Marie-Tooth disease: from genes to phenotypes. J Peripher Nerv Syst 2013;18:113–129.
2. Kabzinska D, Hausmanowa-Petrusewicz I, Kochanski A. Charcot-Marie-Tooth disorders with an autosomal recessive mode of inheritance. Clin Neuropathol 2008;27:1–12.
3. Saporta AS, Sottile SL, Miller LJ, et al. Charcot-Marie-Tooth disease subtypes and genetic testing strategies. Ann Neurol 2011; 69:22–33.
4. Murphy SM, Laura M, Fawcett K, et al. Charcot-Marie-Tooth disease: frequency of genetic subtypes and guidelines for genetic testing. J Neurol Neurosurg Psychiatry 2012;83:706–710.
5. 4th Workshop of the European CMT-Consortium—62nd ENMC International Workshop: rare forms of Charcot-Marie-Tooth disease and related disorders 16–18 October 1998, Soestduinen, The Netherlands. Neuromuscul Disord 1999;9:279–287.
6. Kioussi C, Matsas R. Endopeptidase-24.11, a cell-surface peptidase of central nervous system neurons, is expressed by Schwann cells in the pig peripheral nervous system. J Neurochem 1991;57: 431–440.
7. Kioussi C, Crine P, Matsas R. Endopeptidase-24.11 is suppressed in myelin-forming but not in non-myelin-forming Schwann cells during development of the rat sciatic nerve. Neuroscience 1992; 50:69–83.
8. Turner AJ, Isaac RE, Coates D. The neprilysin (NEP) family of zinc metalloendopeptidases: genomics and function. Bioessays 2001; 23:261–269.
9. Miners JS, Barua N, Kehoe PG, et al. Abeta-degrading enzymes: potential for treatment of Alzheimer disease. J Neuropathol Exp Neurol 2011;70:944–959.
10. Saido TC. Metabolism of amyloid beta peptide and pathogenesis of Alzheimer's disease. Proc Jpn Acad Ser B Phys Biol Sci 2013; 89:321–339.
11. Baranello RJ, Bharani KL, Padmaraju V, et al. Amyloid-beta protein clearance and degradation (ABCD) pathways and their role in Alzheimer's disease. Curr Alzheimer Res 2015;12:32–46.
12. Miners JS, Van Helmond Z, Chalmers K, et al. Decreased expression and activity of neprilysin in Alzheimer disease are associated with cerebral amyloid angiopathy. J Neuropathol Exp Neurol 2006;65:1012–1021.
13. Madani R, Poirier R, Wolfer DP, et al. Lack of neprilysin suffices to generate murine amyloid-like deposits in the brain and behavioral deficit in vivo. J Neurosci Res 2006;84:1871–1878.
14. Zhao Z, Hashiguchi A, Hu J, et al. Alanyl-tRNA synthetase mutation in a family with dominant distal hereditary motor neuropathy. Neurology 2012;78:1644–1649.
15. Tokunaga S, Hashiguchi A, Yoshimura A, et al. Late-onset Charcot-Marie-Tooth disease 4F caused by periaxin gene mutation. Neurogenetics 2012;13:359–365.
16. Nakamura T, Hashiguchi A, Suzuki S, et al. Vincristine exacerbates asymptomatic Charcot-Marie-tooth disease with a novel EGR2 mutation. Neurogenetics 2012;13:77–82.
17. Hashiguchi A, Higuchi Y, Nomura M, et al. Neurofilament light mutation causes hereditary motor and sensory neuropathy with pyramidal signs. J Peripher Nerv Syst 2014;19:311–316.
18. Li H, Durbin R. Fast and accurate short read alignment with Burrows-Wheeler transform. Bioinformatics 2009;25:1754–1760.
19. Li H, Handsaker B, Wysoker A, et al. The Sequence Alignment/ Map format and SAMtools. Bioinformatics 2009;25:2078–2079.
20. Maeda K, Idehara R, Hashiguchi A, et al. A family with distal hereditary motor neuropathy and a K141Q mutation of small heat shock protein HSPB1. Intern Med 2014;53:1655–1658.
21. Adzhubei IA, Schmidt S, Peshkin L, et al. A method and server for predicting damaging missense mutations. Nat Methods 2010;7: 248–249.
22. Kumar P, Henikoff S, Ng PC. Predicting the effects of coding non-synonymous variants on protein function using the SIFT algorithm. Nat Protoc 2009;4:1073–1081.
23. Choi Y, Sims GE, Murphy S, et al. Predicting the functional effect of amino acid substitutions and indels. PLoS One 2012;7:e46688.
24. Folstein MF, Folstein SE, McHugh PR. "Mini-mental state". A practical method for grading the cognitive state of patients for the clinician. J Psychiatr Res 1975;12:189–198.
25. Rosen WG, Mohs RC, Davis KL. A new rating-scale for alzheimers-disease. American Journal of Psychiatry 1984;141:1356–1364.
26. Medical Research Council. Aids to examination of the peripheral nervous system. London: Her Majesty's Stationary Office; 1976;45.
27. Ng SB, Buckingham KJ, Lee C, et al. Exome sequencing identifies the cause of a mendelian disorder. Nat Genet 2010;42:30–35.
28. Ku CS, Cooper DN, Polychronakos C, et al. Exome sequencing: dual role as a discovery and diagnostic tool. Ann Neurol 2012;71:5–14.
29. Montenegro G, Powell E, Huang J, et al. Exome sequencing allows for rapid gene identification in a Charcot-Marie-Tooth family. Ann Neurol 2011;69:464–470.
30. Gilissen C, Hoischen A, Brunner HG, et al. Disease gene identification strategies for exome sequencing. Eur J Hum Genet 2012; 20:490–497.
31. Zhang X. Exome sequencing greatly expedites the progressive research of Mendelian diseases. Front Med 2014;8:42–57..
32. D'Adamio L, Shipp MA, Masteller EL, et al. Organization of the gene encoding common acute lymphoblastic leukemia antigen (neutral endopeptidase 24.11): multiple miniexons and separate 5′ untranslated regions. Proc Natl Acad Sci U S A 1989;86:7103–7107.
33. Roques BP, Noble F, Dauge V, et al. Neutral endopeptidase 24.11: structure, inhibition, and experimental and clinical pharmacology. Pharmacol Rev 1993;45:87–146.
34. Olerud JE, Usui ML, Seckin D, et al. Neutral endopeptidase expression and distribution in human skin and wounds. J Invest Dermatol 1999;112:873–881.
35. Debiec H, Nauta J, Coulet F, et al. Role of truncating mutations in *MME* gene in fetomaternal alloimmunisation and antenatal glomerulopathies. Lancet 2004;364:1252–1259.
36. Tong J, Xie J, Ren H, et al. Comparison of glomerular transcriptome profiles of adult-onset steroid sensitive focal segmental glomerulosclerosis and minimal change disease. PLoS One 2015;10:e0140453.
37. Barnes K, Matsas R, Hooper NM, et al. Endopeptidase-24.11 is striosomally ordered in pig brain and, in contrast to aminopeptidase N and peptidyl dipeptidase A ('angiotensin converting enzyme'), is a marker for a set of striatal efferent fibres. Neuroscience 1988;27:799–817.
38. Barnes K, Doherty S, Turner AJ. Endopeptidase-24.11 is the integral membrane peptidase initiating degradation of somatostatin in the hippocampus. J Neurochem 1995;64:1826–1832.
39. Fukami S, Watanabe K, Iwata N, et al. Abeta-degrading endopeptidase, neprilysin, in mouse brain: synaptic and axonal localization inversely correlating with Abeta pathology. Neurosci Res 2002;43:39–56.
40. Lu B, Gerard NP, Kolakowski LF, Jr, et al. Neutral endopeptidase modulation of septic shock. J Exp Med 1995;181:2271–2275.
41. Lu B, Figini M, Emanueli C, et al. The control of microvascular permeability and blood pressure by neutral endopeptidase. Nat Med 1997;3:904–907.
42. Fischer HS, Zernig G, Schuligoi R, et al. Alterations within the endogenous opioid system in mice with targeted deletion of the neutral endopeptidase ('enkephalinase') gene. Regul Pept 2000; 96:53–58.

43. Iwata N, Tsubuki S, Takaki Y, et al. Identification of the major Abeta1-42-degrading catabolic pathway in brain parenchyma: suppression leads to biochemical and pathological deposition. Nat Med 2000;6:143–150.

44. Iwata N, Tsubuki S, Takaki Y, et al. Metabolic regulation of brain Abeta by neprilysin. Science 2001;292:1550–1552.

45. Iwata N, Higuchi M, Saido TC. Metabolism of amyloid-beta peptide and Alzheimer's disease. Pharmacol Ther 2005;108:129–148.

46. Walther T, Albrecht D, Becker M, et al. Improved learning and memory in aged mice deficient in amyloid beta-degrading neutral endopeptidase. PLoS One 2009;4:e4590.

47. Clarimon J, Munoz FJ, Boada M, et al. Possible increased risk for Alzheimer's disease associated with neprilysin gene. J Neural Transm 2003;110:651–657.

48. Helisalmi S, Hiltunen M, Vepsalainen S, et al. Polymorphisms in neprilysin gene affect the risk of Alzheimer's disease in Finnish patients. J Neurol Neurosurg Psychiatry 2004;75:1746–1748.

49. Vlassenko AG, Benzinger TL, Morris JC. PET amyloid-beta imaging in preclinical Alzheimer's disease. Biochim Biophys Acta 2012; 1822:370–379.

50. Kioussi C, Mamalaki A, Jessen K, et al. Expression of endopeptidase-24.11 (common acute lymphoblastic leukaemia antigen CD10) in the sciatic nerve of the adult rat after lesion and during regeneration. Eur J Neurosci 1995;7:951–961.

51. Kramer HH, He L, Lu B, et al. Increased pain and neurogenic inflammation in mice deficient of neutral endopeptidase. Neurobiol Dis 2009;35:177–183.

52. Ohkushi G, Suzuki N, Kobayashi S, et al. Axonal transport of neprilysin in rat sciatic nerves. J Mol Neurosci 2014;53:96–102.

53. Shy ME, Jani A, Krajewski K, et al. Phenotypic clustering in MPZ mutations. Brain 2004;127:371–384.

54. Iwata N, Sekiguchi M, Hattori Y, et al. Global brain delivery of neprilysin gene by intravascular administration of AAV vector in mice. Sci Rep 2013;3:1472.